Effect of uniform distributions of bonded and debonded fibers on the growth of the fiber/matrix interface crack in UD laminates with different fiber contents under transverse loading

Luca Di Stasio[a,b], Janis Varna[b], Zoubir Ayadi[a]

[a]Université de Lorraine, EEIGM, IJL, 6 Rue Bastien Lepage, F-54010 Nancy, France
[b]Luleå University of Technology, University Campus, SE-97187 Luleå, Sweden

Abstract

Priority: 1

Target journal(s): Composites Part B: Engineering, Composites Part A: Applied Science and Manufacturing, Composite Structures, Journal of Composite Materials, Composite Communications

1. Introduction

1. We start with a few lines devoted to the spread tow technology and thin plies: what they are, what can be done, what are the possible applications.

5   2. By quoting the relevant references, we report on the observation that one of the main beneficial mechanisms in thin ply is the retardation of transverse crack propagation. We then enlarge by reporting the microscopical observations by Saito, in which debonds where also observed. We observe that available microscopic observations are just a few and mainly in 2D.

10   3. Propagation of transverse cracks has been widely investigated both analytically and numerically

4. Initiation at the level of fiber/matrix interface is instead a less researched subject.

2. RVE models & FE discretization

2.1. Introduction & Nomenclature

In order to investigate the interaction between debonds in UD composites, we developed different models of laminates in which the only damage present is represented by the fiber/matrix interface crack. All of these Representative Volume Elements feature regular microstructures with fibers placed according to a square-packing tiling. As the very high longitudinal modulus of UD composites and cross-ply laminates ensures that the y-strain due to loading in the x-direction is small, we consider only 2D models under the assumption of plane strain, defined in the $x - z$ section of the laminate. Consequently, debonds are considered to be significantly longer in the fiber direction than in the arc direction. The analysis presented thus applies to long debonds, of which we are interested in understanding the mechanisms of growth along its arc direction. The UD composites are further supposed to be subjected to transverse

2

tension, applied along the x direction in the pictures. As the models are differentiated by the number of layers of fibers and by the spacing between debonds along the vertical and horizontal directions, we introduce the common notation

45    $D\left(m+1\right)H\left(k+1\right)V\left(2p+1\right)L$ which stands for: *a **D**ebond every* $\left(m+1\right)^{th}$ *fiber in the **H**orizontal direction and every* $\left(k+1\right)^{th}$ *fiber in the **V**ertical direction, in a UD composites with* $\left(2p+1\right)^{th}$ ***L**ayers of fibers.* The exact meaning of the parameters m, k, and p will become clearer in Section 2.2.

2.2. Models of Representative Volume Element (RVE)

50   The first two models feature, as shown in Fig. 1, a UD laminate with only one layer of fibers across its thickness. This is quite an extreme model from the microstructural point of view; however, it allows to focus the analysis on the interaction between debonds placed along the direction of the load. Furthermore, as the upper surface is considered free, the interaction is stronger in this case

55   than in any other, making the predictions of this model rather conservative. In retrospective, if only 20 years ago such a model would have been considered too abstracted from the physical reality, the recent advancements in the spread tow technology make this approach appealing also for practical considerations.

(a) Single layer of fibers with a debond appearing every m fibers.

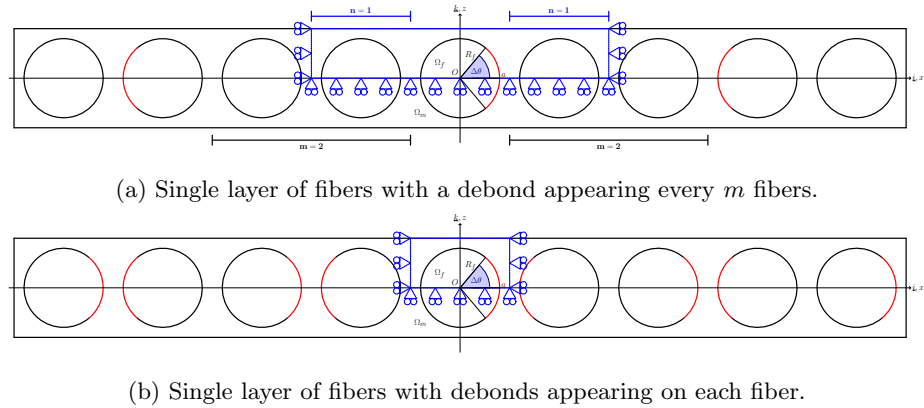(b) Single layer of fibers with debonds appearing on each fiber.

Figure 1: Models of UD laminates with a single layer of fibers and debonds repeating at different distances. The corresponding repeating element (RVE) is highlighted in blue.

In the first version of the model laminate, Fig. 1a, debonds appear in the

3

laminate on every $(m+1)^{th}$ fiber on alternating sides of the partially debonded fiber. The symmetries of the model allow the use of a Repeating Unit Cell (RUC), which corresponds to the Representative Volume Element (RVE) of this microstructure, with a central debonded fiber and $n = \frac{m}{2}$ fiber(s) on each side. It is highlighted by blue lines in 1a. Symmetry is applied on the lower boundary and kinematic coupling conditions on the left and right sides. As mentioned, the upper surface is left free. Following the notation introduced in Section 2.1, we will refer to this model as $D(m+1)H0V1L$, where $k = -1, p = 0$. In the second version of the single-layer-of-fibers model, 1b, a debond appears on each fiber on alternating sides. The corresponding RUC has only one debonded fiber, with symmetry on the lower side and kinematic coupling on the left and right ones. The upper boundary is again free. We will refer to this model as $D1H0V1L$, where $k = -1, m = p = 0$.

The second set of models considers instead laminates with multiple layers of fibers across the thickness: a finite number of layers in the first two models (2a and 2b); an infinite number in the model of Fig. 3. In the first model (Fig. 2a) all the fibers in the central layer are debonded. The UD is made by $2p+1$ layers of fibers across the thickness, corresponding to a RUC with $q = p$ fibers above. This model will be referred to in the following as $D1H0V(2p+1)L$, where $k = -1, m = 0$. In the second model (Fig. 2b), a debond appear every $(m+1)^{th}$ fiber in the central line of fibers in a laminate with $2p+1$ layers. The corresponding RUC has thus $n = \frac{m}{2}$ fiber(s) on each side and $q = p$ above. We will refer to this model as $D(m+1)H0V(2p+1)L$, where $k = -1$.

Finally, the last model considers an UD composite with an infinite number of partially debonded fibers. The corresponding RUC is made by a single fiber with a debond and kinematic coupling conditions applied to the upper boundary. This model is referred to as $D1H1V\infty L$, where $m = k = 0, p \to \infty$. For all these last three models, the corresponding RUC possesses symmetry on the lower boundary, and kinematic coupling is applied on the left and right sides.

A summary of models' names and characteristics is reported in Table 1

4
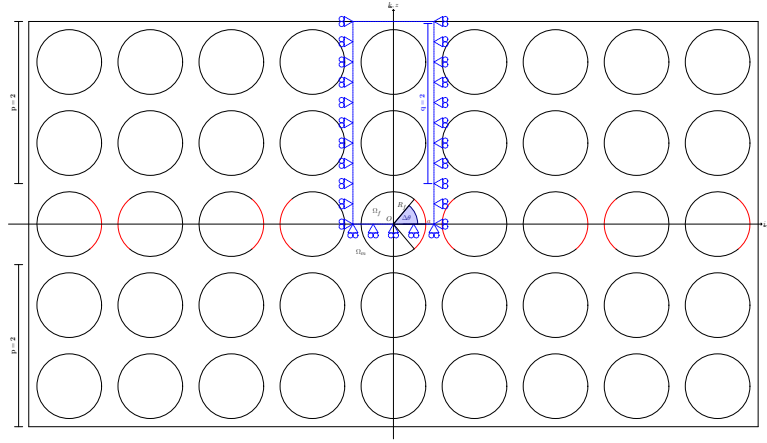
(a) Multiple layers of fibers with debonds appearing on each fiber beloging to the central layer.
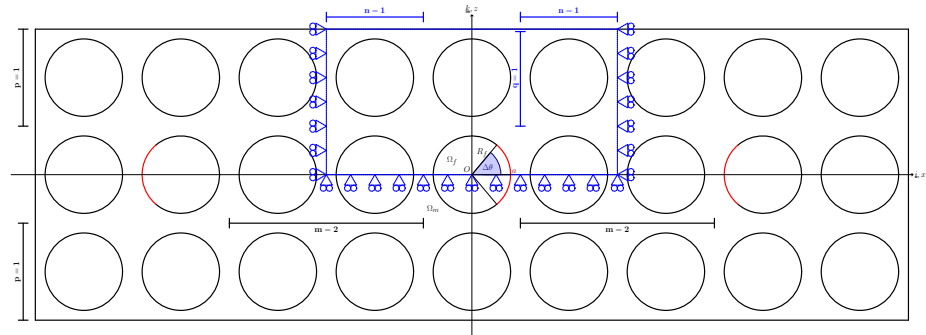
(b) Mutiple layers of fibers with a debond appearing every m fibers within the central layer.

Figure 2: Models of UD laminates with different layers of fibers and debonds repeating at different distances. The corresponding repeating element (RVE) is highlighted in blue.

2.3. Finite Element (FE) discretization

Each RUC is discretized using the Finite Element Method (FEM) within the Abaqus environment, a commercial FEM package [1]. The length l and height h of the model (see Fig. 4a) are determined by number of fibers n present on the side and the number of layers q above the central line of fibers (see 2.2) according to Eq. 1:
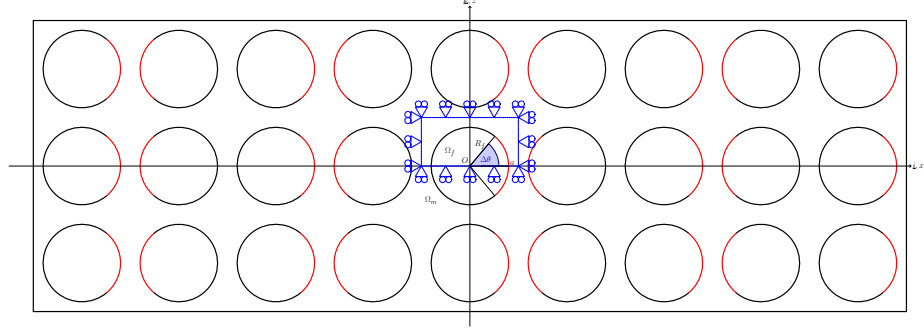
5

Figure 3: Model of UD laminates with an infinite number of layers of fibers and debonds appearing on each fiber. The corresponding repeating element (RVE) is highlighted in blue.

$$l = (2n + 1) L \qquad h = (2q + 1) L; \tag{1}$$

where the reference length L is defined as a function of the fiber volume fraction V_f and the fibers' radius according to

$$L = \frac{R_f}{2} \sqrt{\frac{\pi}{V_f}}. \tag{2}$$

The fibers' radius R_f is assumed to be the same for each fiber present n the model and equal to $1\mu m$. The relationships in Eqs. 1 and 2 thus ensure that the local and global V_f are everywhere equal.
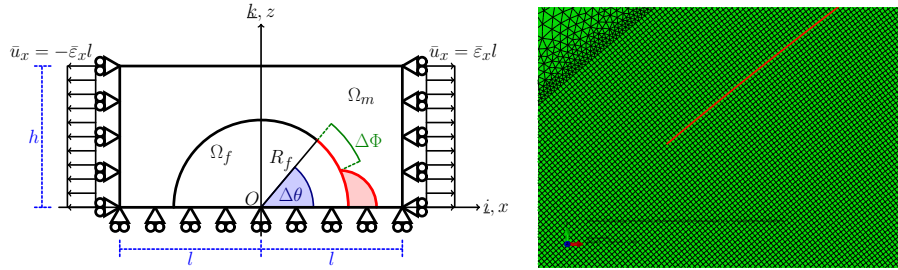
(a) Schematic of the model with its main parameters.

(b) Mesh near the crack tip. Crack's faces shown in red.

Figure 4: Details and main parameters of the Finite Element model.

The debond is placed symmetrically with respect to the x axis (in red in 4a)

Table 1: Summary of the models and their characteristics.

Name	Boundary conditions			
	Up	Down	Right	Left
D $(\mathbf{m+1})$ H0V1L	x-symmetry	free	coupling, $\bar{\varepsilon}_x = 1\%$	coupling, $\bar{\varepsilon}_x = 1\%$
A debond every $(m+1)^{th}$ fiber in the horizontal direction, in a UD composites with 1 layer of fibers, Fig. 1a.				
D1H0V1L	x-symmetry	free	coupling, $\bar{\varepsilon}_x = 1\%$	coupling, $\bar{\varepsilon}_x = 1\%$
A debond every 1st fiber in the horizontal direction, in a UD composites with 1 layer of fibers, Fig. 1b.				
D1H0V $(\mathbf{2p+1})$ L	x-symmetry	free	coupling, $\bar{\varepsilon}_x = 1\%$	coupling, $\bar{\varepsilon}_x = 1\%$
A debond every 1st fiber in the horizontal direction, in a UD composites with $(2p+1)$ layer of fibers, Fig. 2a.				
D $(\mathbf{m+1})$ H0V $(\mathbf{2p+1})$ L	x-symmetry	free	coupling, $\bar{\varepsilon}_x = 1\%$	coupling, $\bar{\varepsilon}_x = 1\%$
A debond every $(m+1)^{th}$ fiber in the horizontal direction, in a UD composites with $(2p+1)$ layers of fibers, Fig. 2b.				
D1H1V∞L	x-symmetry	coupling	coupling, $\bar{\varepsilon}_x = 1\%$	coupling, $\bar{\varepsilon}_x = 1\%$
A debond every 1st fiber in the horizontal direction and every 1st fiber in the vertical direction, in a UD composites with an infinite number of layers of fibers, Fig. 3.				

and has an angular size of $\Delta\theta$ (the full debond's size is thus $2\Delta\theta$). For high debond's sizes ($\geq 60° - 80°$), a region of variable size $\Delta\Phi$ appears at the crack tip in which the crack's faces are in contact and slide on each other. Due to its appearance, frictionless contact is considered between the two crack's faces

7

to allow free slipping and avoid interpenetration. Symmetry with respect to the x axis is applied on the lower boundary and kinematic coupling on the left and right sides. The upper boundary is in general free, except for the model $D1H1V\infty L$ (Fig. 3) which requires kinematic coupling also on the upper side. Constant transverse strain $\bar{\varepsilon}$ equal to 1% is applied to the right and left sides by means of an imposed displacement of, respectively, $\pm\bar{\varepsilon}l$.

Table 2: Summary of the mechanical properties of fiber and matrix.

Material	$E\,[GPa]$	$G\,[GPa]$	$\nu\,[-]$
Glass fiber	70.0	29.2	0.2
Epoxy	3.5	1.25	0.4

The model is meshed using second order, 2D, plane strain triangular (CPE6) and rectangular (CPE8) elements. A regular mesh of quadrilateral elements with an almost unitary aspect ratio is required at the crack tip, as shown in Fig. 4b. The angular size δ of an element in the crack tip region is always equal to 0.05°. The mode I, mode II and total Energy Release Rates (ERRs) represent the main output of the FEM analysis; they are evaluated using the VCCT technique [2] implemented in a custom Python routine and, for the total ERR, the J-integral [3] by application of the Abaqus built-in functionality. A glass fiber-epoxy system is considered in every model, and it is assumed that their response lies always in the linear elastic domain. The properties used are listed in Table 2.

2.4. Validation of the model

The model is validated in Fig. 5 against the results reported in [4], obtained with the Boundary Element Method (BEM) for a single fiber with a symmetric debond placed in an infinite matrix. This situation is modeled using the *free* RVE with $V_f = 0.0079\%$, which corresponds to a RUC's length and height of ~ 100.
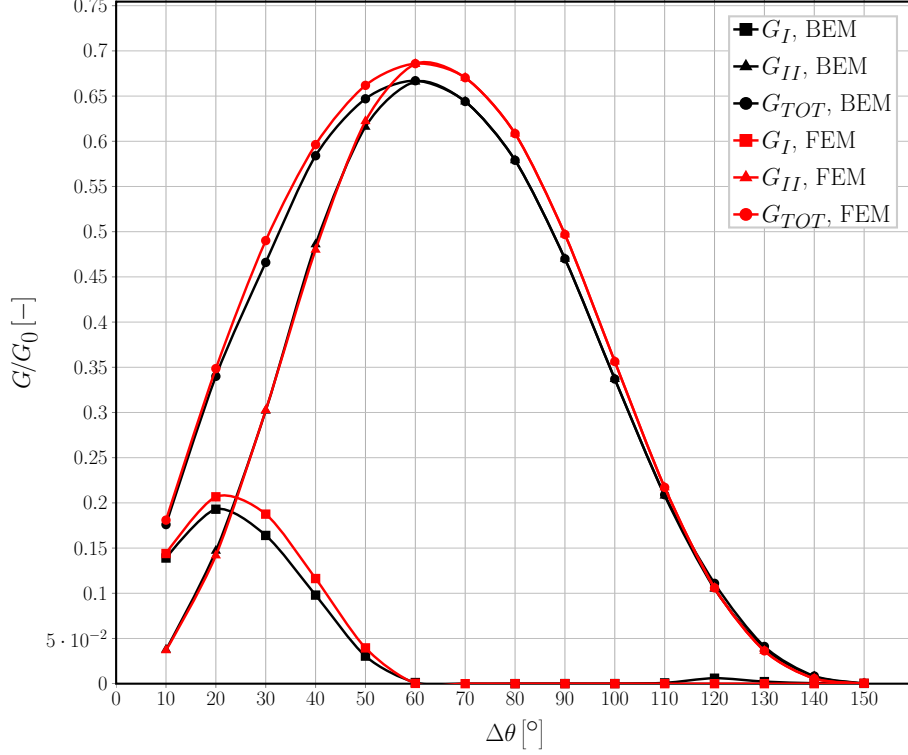
Figure 5: Validation of the single fiber model for the infinite matrix case with respect to the BEM solution in [4].

To allow for a comparison, the results are normalized following [4] with respect to a reference Energy Release Rate G_0 defined as

$$G_0 = \frac{1 + k_m}{8\mu_m} \sigma_0^2 \pi R_f \tag{3}$$

where μ is the shear modulus, k_m is the Kolosov's constant defined as $3 - 4\nu$ for plane strain conditions, R_f is the fiber radius and the pedix m refers to the properties of the matrix. σ_0 is the stress at the boundary, computed as the average of the stress extracted at each boundary node along the right side (arithmetic average as nodes are equispaced by design along both the left and right sides).

3. Results & Discussion

3.1. Effect of Fiber Volume Fraction

As shown in Figs. 6 and 7, respectively for mode I and mode II, the fiber content has a drastic effect on the Energy Release Rate at the crack tip of the fibre/matrix interface crack. The effect of four levels of fiber volume fraction are compared, 30%, 50%, 60% and 65%, on two microstructural models: a D6H0V11L (a debond every 6th fiber in the central layer of an UD with 11 layers of fibers), Figs. 6a and 7a, and a D11H0V21L (a debond every 11th fiber in the central layer of an UD with 21 layers of fibers), Figs. 6b and 7b.

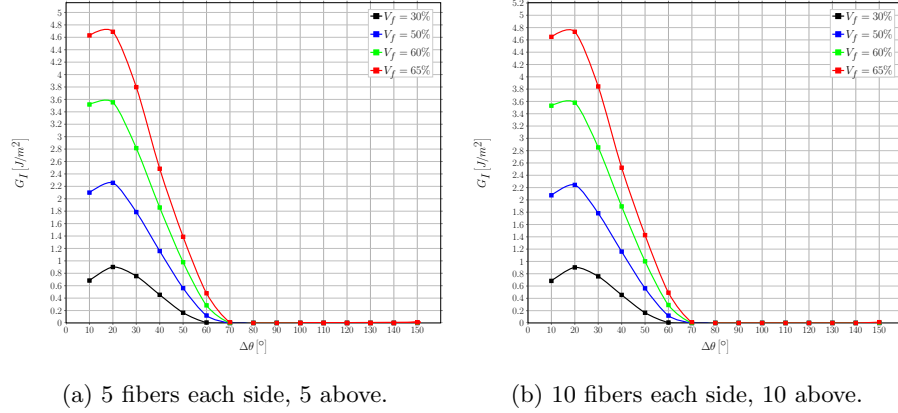(a) 5 fibers each side, 5 above.   (b) 10 fibers each side, 10 above.

Figure 6: A view of the effect of fiber volume fraction on Mode I ERR in two exemplificative models.

Comparison of Fig. 6a with 6b, and of of Fig. 7a with 7b, indicates that there exists a specific effect of the fiber content, independent of the microstructure. For mode I, Fig. 6, the maximum value of the ERR is increased by ~ 5.2 times when V_f changes from 30% to 65% in both models. The debond's size for which the peak value occurs remains unchanged at 20°, but for 60% and 65% the value at 10° and at 20° are almost identical, approximately creating a plateau and thus making the growth of small debonds ($\leq 20°$) in mode I unstable. Furthermore, increasing the fiber volume fraction delays the onset of the contact zone, which corresponds in 6 to the first value of $\Delta\theta$ for which G_I is equal. For $V_f = 30\%$,

10

the contact zone first appears for a debond of 60°, similarly to what happens in the single fiber in infinite matrix modle (Fig. 5). For higher fiber contents, the contact zone's onset is delayed to a debond's size equal to 70°.

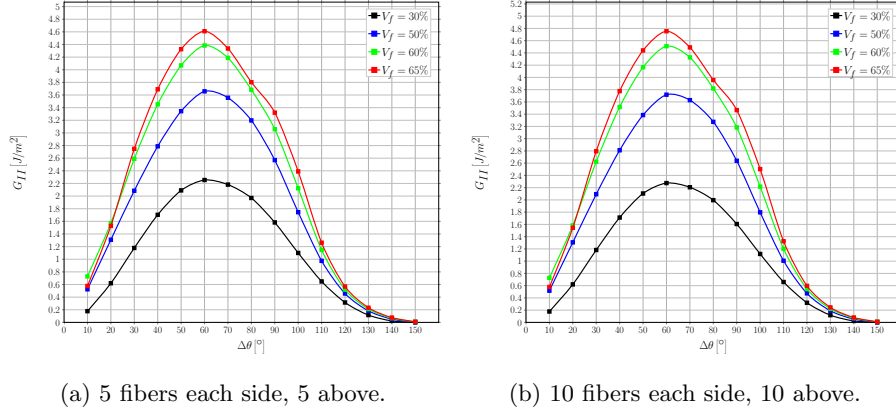(a) 5 fibers each side, 5 above.   (b) 10 fibers each side, 10 above.

Figure 7: A view of the effect of fiber volume fraction on Mode II ERR in two exemplificative models.

For mode II, Fig. 6, the maximum value of the ERR is increased by ~ 2.1 times when V_f changes from 30% to 65% in both models. The effect is thus similar to mode I, but with a significantly lower magnitude. As for mode I, the debond's size for which the peak value occurs remains unchanged, at 60° for mode II. The shape of the curve remains instead unchanged, thus no effect on the stability of mode II with respect to debond's size can be observed. It is worthwhile to notice, however, that the ratio of mode II to mode I peak values is $\frac{max(G_{II})}{max(G_I)} \sim \frac{2.2}{0.9} \sim 2.4$ for $V_f = 30\%$, while it is $\sim \frac{4.7}{4.7} \sim 1$ for $V_f = 65\%$ in both models. Given that the peaks occur at different debond's sizes, for which the value of the other ERR is very small or even close to zero, this means that the increase in fiber content creates a long range of very close values of total ERR, and thus has a global destabilizing effect on the debond's growth.

The general incresing trends observed in Figs. 6 and 7 are related to the fact that, given that the global and local V_f are everywhere identical in the models presented, an increase in fiber content corresponds to a decrease in the average distance between fibers. Thus, the relaxation of the stress and strain fields in

11

the matrix domain occurs over smaller lengths causing higher values at the crack

¹⁷⁵ tip. The difference in relative magnification between mode I and mode II and the delay in the contact zone's onset are instead due to the interplay between two different mechanisms, both caused by ordered microstructural arrangement of the model. In the models considered, a fully bonded fiber is always placed along the horizontal direction, aligned with the partially debonded fiber and

¹⁸⁰ exactly in front of the debond. By increasing V_f, the former moves closer to the latter and this causes a magnification of the x-strain at the crack tip. For small debonds ($\leq 20° - 30°$), the crack tip is approximately normal to the x-direction and thus an increase in ε_x causes an increase in G_I. On the other hand, for large debonds ($\geq 70° - 80°$) the crack growth is almost aligned with the x-axis,

¹⁸⁵ thus a magnification in the x-strain translates into an increase of mode II ERR. However, this increasing effect on G_{II} is counteracted by the presence of a fully bonded fiber along the vertical direction, aligned with the partially debonded one. As fibers are more rigid than the sourrounding matrix, the presence of the former will restrain horizontal displacements, thus hampering strong increases in

¹⁹⁰ G_{II} for large debonds. Furthermore, due to the mismatch in the Poisson's ratios, the fully bonded fiber placed above generates an upward-directed component of the vertical displacement field in the matrix, which tends to open the debond and causes the delay in the contact zone's onset. The interplay between these mechanisms is governed by the average inter-fiber distance and, in turn, by the

¹⁹⁵ fiber volume fraction.

3.2. Interaction between debonds in UD laminates with a single layer of fibers

The interaction of debonds appearing at regular intervals in UD composites with a single layer of fibers is studied for mode I (Fig. 8) and mode II (Fig. 9) and fiber content equal to 30% (Figs. 8a and 9a) and 60% (Figs. 8b and 9b). The

²⁰⁰ models treated are $D3H0V1L$, $D5H0V1L$, $D7H0V1L$, $D11H0V1L$, $D21H0V1L$, $D101H0V1L$ and $D201H0V1L$, corresponding respectively to a debond every 3rd, 5th, 7th, 11th, 21st, 101st and 201st fiber (Fig. 1a). Given that the upper surface of the UD is left free, the interaction is stronger than in any other

12

case and the results of this section are thus the most conservative in terms of debond's growth. From both 8 and 9, it can be seen that the presence of a debond decreases the strain magnification effect discussed in Sec. 3.1 and thus reduces the value of the ERR.
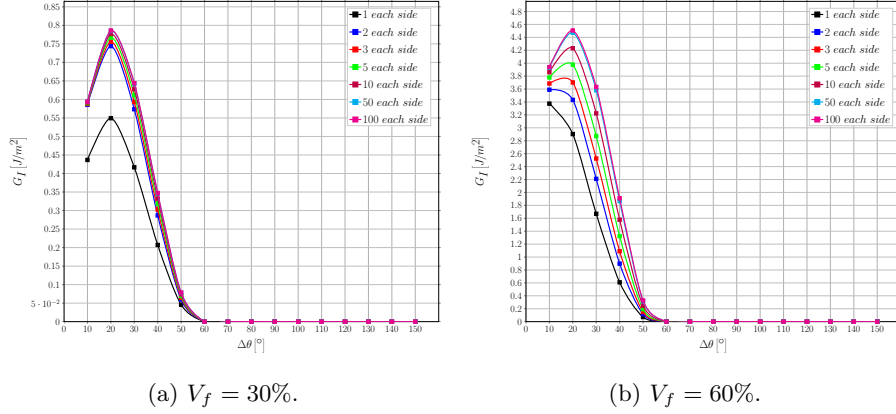

(a) $V_f = 30\%$.

(b) $V_f = 60\%$.

Figure 8: Effect of the interaction between debonds appearing at regular intervals on Mode I ERR in an UD with a single layer of fibers at different levels of fiber volume fraction V_f.

For mode I, the presence of a free surface, and inversely the absence of a fully bonded fiber along the vertical direction, implies the absence of the counteracting upward-oriented vertical component of the displacement field due to the mismatch in Poisson's ratios. This in turn translates into the constancy of the value of $\Delta\theta$ corresponding to contact zone's onset, always equal to $60°$. For $V_f = 30\%$, mode I is reduced going from a debond placed every 5th fiber to every 3th fiber. Larger spacing does not seem to have a sizable effect. Similarly, at 60% no difference can be seen between the case of a debond placed every 101th and every 201th fiber. These observations suggest the existence of characteristic distance dependent on the fiber volume fraction which governs the interaction between debonds.

Without costraint on the upper surface, the strain magnification effect creates larger displacements in the x-direction, which increase mode II for larger debonds. When debonds are far apart, the series of rigid elements (constituted by fully bonded fibers and their sorronding matrix) creates higher x-strains,
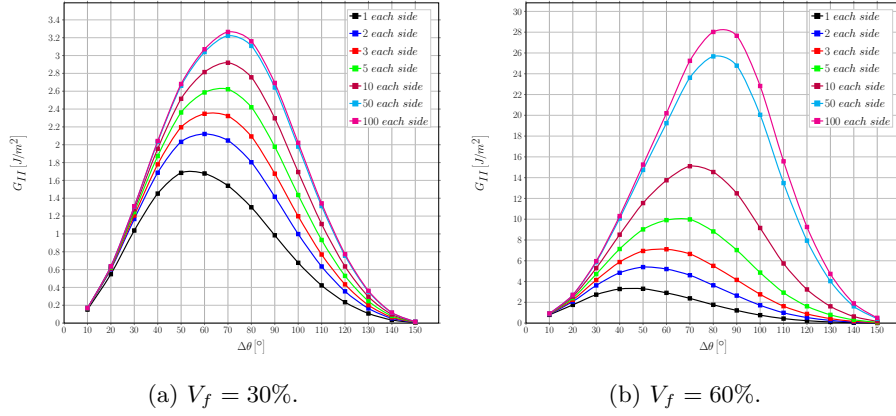
13

Figure 9: Effect of the interaction between debonds appearing at regular intervals on Mode II ERR in a single-ply laminate with a single layer of fibers at different levels of fiber volume fraction V_f.

which in turn generates higher tangential displacements at the crack tip for larger debonds. Conversely, when debonds are closer, the strain concentration is reduced and the tangential component at the crack tip decreases for large $\Delta\theta$. This is the mechanism behind the change in the value of $\Delta\theta$ for which the peak of G_{II} occurs: from $70°$ to $50°$ at 30%, and from $80°$ to $40°$ at 60% going from the higher to the smaller spacing of debonds. Differently from mode I, the presence of a characteristic distance is harder to establish. For $V_f = 30\%$ (Fig. 9a), it seems reasonable to establish it at around 100 fully bonded fibers between each debond. For $V_f = 60\%$ (Fig. 9b), the difference between models $D101H0V1L$ and $D201H0V1L$ is still sizable, thus preventing the establishment of such characteristic distance. It is possible to observe, however, that the change between $D101H0V1L$ and $D201H0V1L$ is significantly smaller than between $D21H0V1L$ and $D101H0V1L$ ($2 \left[\frac{J}{m^2}\right]$ vs $11 \left[\frac{J}{m^2}\right]$), thus suggesting the existence of the characteristic distance outside the range studied.

14

3.3. Influence of layers of fully bonded fibers on debond's growth in a line of debonded fibers located at mid-thickness

The effect of the presence of layers of fully bonded fibers on debond's growth
²⁴⁰ in a line of partially debonded fibers located at mid-thickness in UD composites
is studied for mode I (Fig. 10) and mode II (Fig. 11) and fiber content equal to
30% (Figs. 10a and 11a) and 60% (Figs. 10b and 11b). The models treated are
$D1H0V3L$, $D1H0V5L$, $D1H0V7L$, $D1H0V11L$, $D1H0V21L$, $D1H0V101L$
and $D1H0V201L$, corresponding to a debond every 1st fiber in the horizontal
²⁴⁵ direction, in a UD composites with respectively 3, 5, 7, 11, 21, 101 and 201
layers of fibers (Fig. 2a).

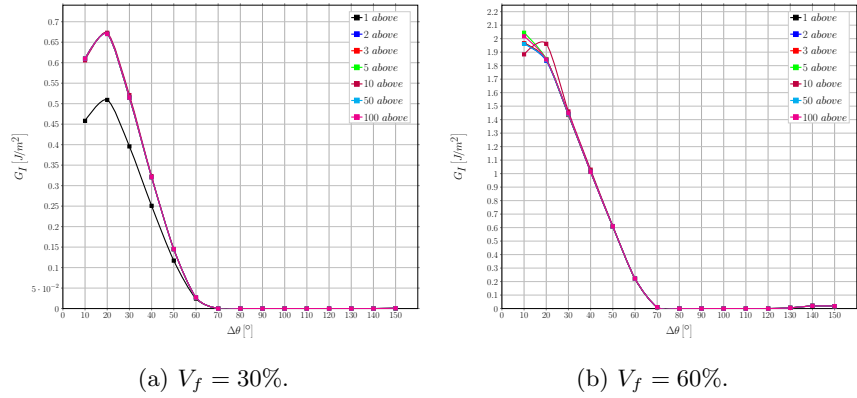(a) $V_f = 30\%$.   (b) $V_f = 60\%$.

Figure 10: Influence of layers of fully bonded fibers on debond's growth in Mode I ERR in a centrally located line of debonded fibers at different levels of fiber volume fraction V_f.

3.4. Interaction between debonds in UD laminates with multiple layers of fibers

Finally models that are closer to real laminates and are more complex (2
parameters: number of fibers along the horizontal direction, number of layers
²⁵⁰ in the vertical one). G_I in Fig. 12, G_{II} in Fig. 13.

One graphic for each V_f (30%,50%,60%,65%), one curve for some selected
case of fibers on top and on the side. Hypothesis of selected cases ([n. on side,
n. on top]): [1,1], [2,1], [2,2], [5,1], [5,5], [10,1], [10,10], [50,1], [50,10], [100,1],
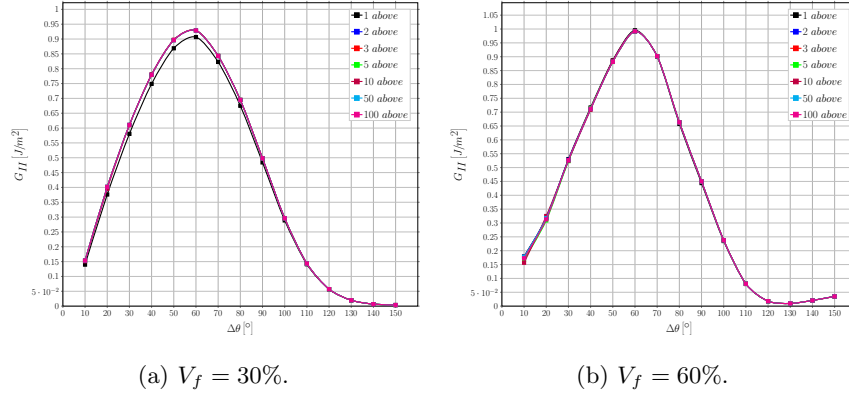
(a) $V_f = 30\%$.

(b) $V_f = 60\%$.

Figure 11: Influence of layers of fully bonded fibers on debond's growth in Mode II ERR in a centrally located line of debonded fibers at different levels of fiber volume fraction V_f.

[100,10]

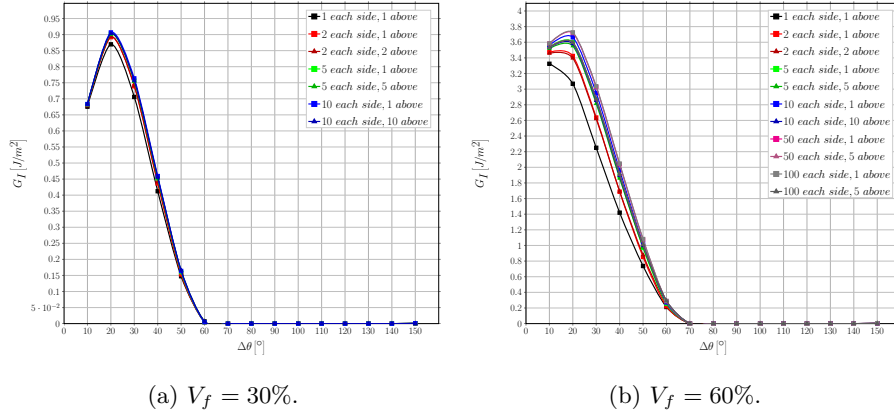255

(a) $V_f = 30\%$.

(b) $V_f = 60\%$.

Figure 12: Effect of the interaction between debonds appearing at regular intervals on Mode I ERR in a single-ply laminate with multiple layers of fibers at different levels of fiber volume fraction V_f.

3.5. Comparison with the single fiber model with equivalent boundary conditions

We compare the previous results with the corresponding models of single fibers with equivalent BC. We draw conclusions on the possibility of using a single fiber with equivalent BCs. By remembering the actual ply configurations
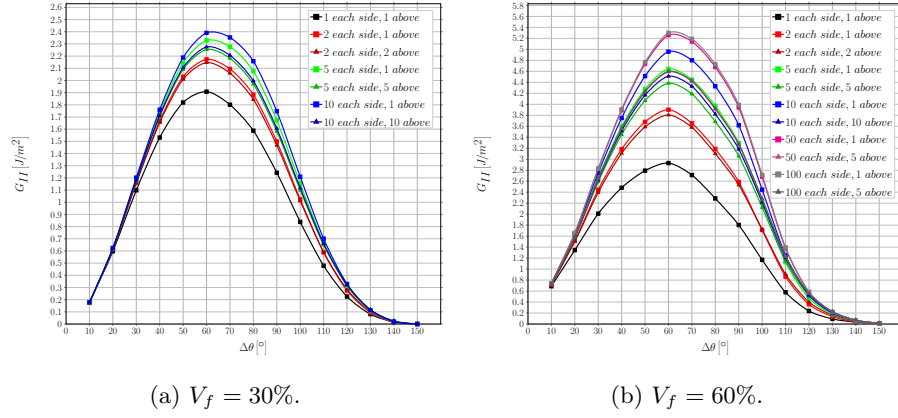
16

(a) $V_f = 30\%$.

(b) $V_f = 60\%$.

Figure 13: Effect of the interaction between debonds appearing at regular intervals on Mode II ERR in a single-ply laminate with multiple layers of fibers at different levels of fiber volume fraction V_f.

the repeating elements are modeling, and observing that in the vertical direction no significant effect related to the presence of debonded or bonded fiber can be found, we conclude that debonds appearing in fibers aligned in the vertical direction are energetically equivalent, and thus different configurations of debonded/bonded fibers along the vertical direction have the same probability. It is thus likely, from the energetic point of view, that debonds form at the same time along fibers aligned vertically. G_I in Fig. 14 and Fig. 16, G_{II} in Fig. 15 and Fig. 17.

One graphic for each V_f (30%,50%,60%,65%), one curve for single fiber with BC + some selected case of fibers on top and on the side. Hypothesis of selected cases ([n. on side, n. on top]): [1,1], [2,1], [2,2], [5,1], [5,5], [10,1], [10,10]
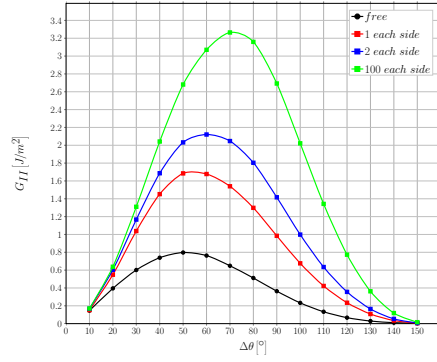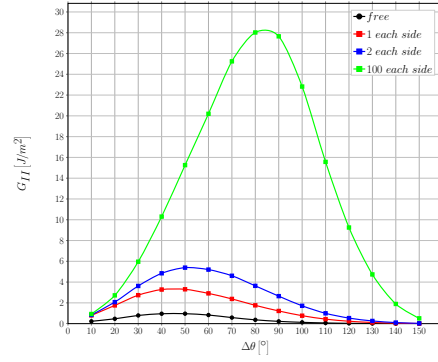
17
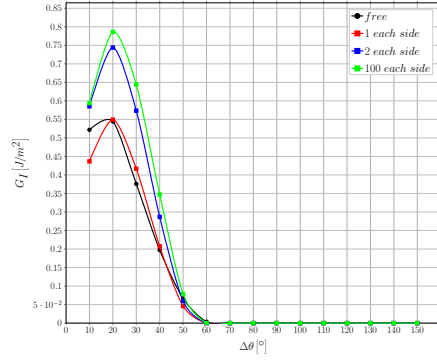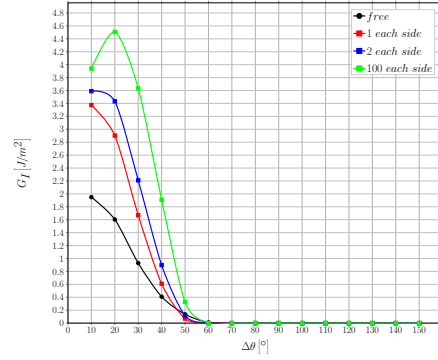
(a) $V_f = 30\%$.

(b) $V_f = 60\%$.

Figure 14: Comparison of Mode I ERR between the single fiber model with free upper boundary and the multiple fibers model with fibers only on the side at different levels of fiber volume fraction V_f.

(a) $V_f = 30\%$.

(b) $V_f = 60\%$.

Figure 15: Comparison of Mode II ERR between the single fiber model with free upper boundary and the multiple fibers model with fibers only on the side at different levels of fiber volume fraction V_f.
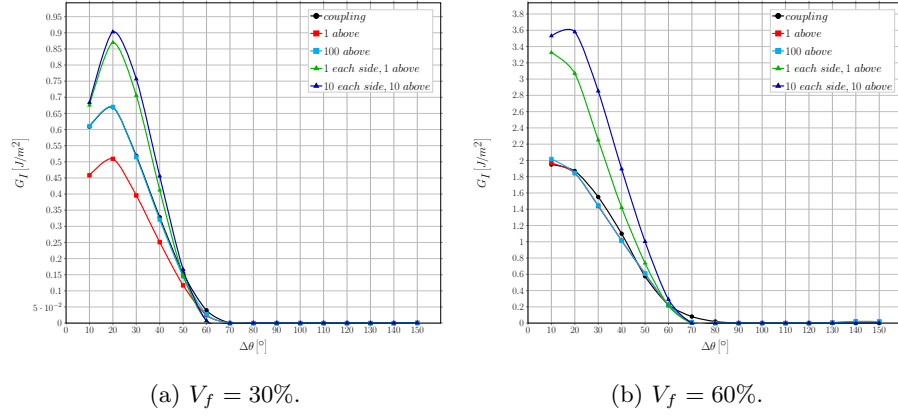
(a) $V_f = 30\%$.   (b) $V_f = 60\%$.

Figure 16: Comparison of Mode I ERR between the single fiber model with coupling conditions along the upper boundary and the multiple fibers model with fibers above and both above and on the side at different levels of fiber volume fraction V_f.
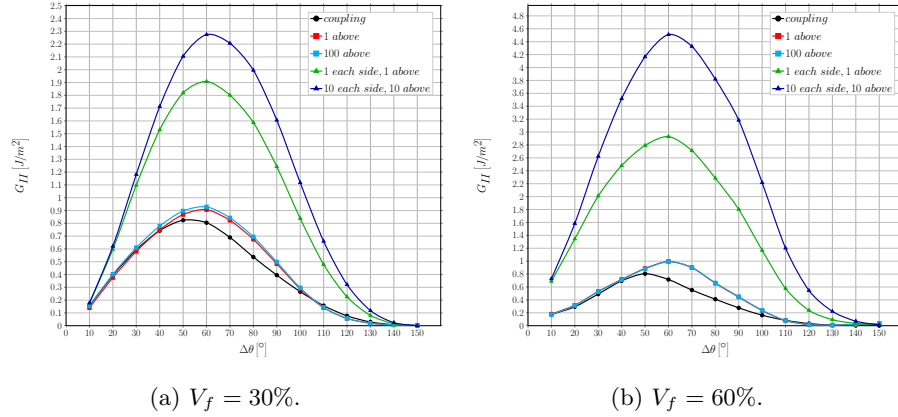

(a) $V_f = 30\%$.   (b) $V_f = 60\%$.

Figure 17: Comparison of Mode II ERR between the single fiber model with coupling conditions along the upper boundary and the multiple fibers model with fibers above and both above and on the side at different levels of fiber volume fraction V_f.

4. Conclusions & Outlook

Acknowledgements

References

[1] Simulia, Providence, RI, USA, ABAQUS/Standard User's Manual, Version 6.12 (2012).

[2] R. Krueger, Virtual crack closure technique: History, approach, and applications, Applied Mechanics Reviews 57 (2) (2004) 109. `doi:10.1115/1.1595677`.

₂₈₀ URL `https://doi.org/10.1115/1.1595677`

[3] J. R. Rice, A path independent integral and the approximate analysis of strain concentration by notches and cracks, Journal of Applied Mechanics 35 (2) (1968) 379. `doi:10.1115/1.3601206`.
URL `https://doi.org/10.1115/1.3601206`

₂₈₅ [4] C. Sandino, E. Correa, F. París, Numerical analysis of the influence of a nearby fibre on the interface crack growth in composites under transverse tensile load, Engineering Fracture Mechanics 168 (2016) 58–75. `doi:10.1016/j.engfracmech.2016.01.022`.
URL `https://doi.org/10.1016/j.engfracmech.2016.01.022`